

Carderock Division
Naval Surface Warfare Center

W. Bethesda, MD 20817-5700

NSWCCD-72--TR-2004/022 February 2004

Signatures Directorate
Research and Development Report

**Leading Edge Surface Pressures from Airfoils in a
Turbulent Flow**

By:

Jonathan L. Gershfeld, NSWCCD 725

Thomas C. Mathews, NSWCCD 725

Approved for public release; Distribution is unlimited.

20040804 070

NSWCCD-72--TR-2004/022 February 2004

Leading Edge Surface Pressures from Airfoils in a Turbulent Flow

REPORT DOCUMENTATION PAGE

Form Approved
OMB No. 0704-0188

Public reporting burden for this collection of information is estimated to average 1 hour per response, including the time for reviewing instructions, searching existing data sources, gathering and maintaining the data needed, and completing and reviewing this collection of information. Send comments regarding this burden estimate or any other aspect of this collection of information, including suggestions for reducing this burden to Department of Defense, Washington Headquarters Services, Directorate for Information Operations and Reports (0704-0188), 1215 Jefferson Davis Highway, Suite 1204, Arlington, VA 22202-4302. Respondents should be aware that notwithstanding any other provision of law, no person shall be subject to any penalty for failing to comply with a collection of information if it does not display a currently valid OMB control number. PLEASE DO NOT RETURN YOUR FORM TO THE ABOVE ADDRESS.

1. REPORT DATE (DD-MM-YYYY) 29-Feb-2004		2. REPORT TYPE Final		3. DATES COVERED (From - To) 1-Dec-2003 - 29-Feb-2004	
4. TITLE AND SUBTITLE Leading Edge Surface Pressures from Airfoils in a Turbulent Flow				5a. CONTRACT NUMBER N0001401WX20236	
				5b. GRANT NUMBER	
				5c. PROGRAM ELEMENT NUMBER 0603561N	
6. AUTHOR(S) Jonathan L. Gershfeld and Thomas C. Mathews				5d. PROJECT NUMBER N/A	
				5e. TASK NUMBER S2033	
				5f. WORK UNIT NUMBER	
7. PERFORMING ORGANIZATION NAME(S) AND ADDRESS(ES) AND ADDRESS(ES) Naval Surface Warfare Center Carderock Division 9500 Macarthur Boulevard West Bethesda, MD 20817-5700				8. PERFORMING ORGANIZATION REPORT NUMBER NSWCCD-72--TR-2004/022	
9. SPONSORING / MONITORING AGENCY NAME(S) AND ADDRESS(ES) Commander Naval Sea Systems Command Code 92R 2531 Jefferson Davis Highway Arlington, VA 22242-5160				10. SPONSOR/MONITOR'S ACRONYM(S)	
				11. SPONSOR/MONITOR'S REPORT NUMBER(S)	
12. DISTRIBUTION / AVAILABILITY STATEMENT Approved for public release; Distribution is unlimited.					
13. SUPPLEMENTARY NOTES					
14. ABSTRACT Surface pressure cross spectral measurements near the leading edges of a variety of airfoils in a turbulent flow disclose contributions from the near fields of the diffracted pressures and the incident pressures from the grid-generated turbulence. The thickness dependence of the measured cross spectra of the near field components of the diffracted surface pressures corresponds to the thickness dependence of the dipole sound measured in the far field.					
15. SUBJECT TERMS airfoils, turbulent flow, diffracted pressures, incident pressures, dipole sound, blade vortex interaction, leading edge shapes					
16. SECURITY CLASSIFICATION OF:			17. LIMITATION OF ABSTRACT UL	18. NUMBER OF PAGES 40	19a. NAME OF RESPONSIBLE PERSON Jonathan L. Gershfeld
a. REPORT UNCLASSIFIED	b. ABSTRACT UNCLASSIFIED	c. THIS PAGE UNCLASSIFIED			19b. TELEPHONE NUMBER (include area code) 301-227-5783

CONTENTS

	Page
ABSTRACT.....	1
ADMINISTRATIVE INFORMATION	1
1. INTRODUCTION	2
2. EXPERIMENT DESIGN.....	7
3. EXPERIMENTAL RESULTS.....	15
4. CONCLUSIONS.....	32
REFERENCES	33

FIGURES

1.1	A comparison of the NACA 0012 ($h/c=0.12$) dipole sound measurements of Paterson and Amiet (1976,1977) (points), and the thickness theory [Eq. (3.8) of Gershfeld (2003)] with $h/c=0.0$ (lines) for flow speeds of 40 m/s, 60 m/s, 90 m/s, and 120 m/s.	5
1.2	A comparison of the NACA 0012 ($h/c=0.12$) dipole sound measurements of Paterson and Amiet (1976, 1977) (points), and the thickness theory [Eq. (3.8) of Gershfeld (2003)] with $h/c = 0.12$ (lines) for flow speeds of 40 m/s, 60 m/s, 90 m/s, and 120 m/s.	6
2.1	Anechoic flow facility, NSWCCD	9
2.2	An illustration of the turbulence generating bi-plane grid design.	10
2.3	Experimental configuration of turbulence generating grid and airfoil in the Anechoic Flow Facility.....	11
2.4	A comparison of dimensionless parameters of Paterson and Amiet (1976) and the current experiment	12
2.5	Schematic of a NACA foil section shape oriented with the leading edge or round nose (RN) facing the wind and with the trailing edge or sharp nose (SN) facing the wind.	13
2.6	Illustrations of the wedge nose (WN) and round nose (RN) geometry	14
3.1	Coherence functions, $\gamma(\omega y/U)$ for sharp nose (SN) and round nose (RN) leading edges obtained from surface pressures measured on opposite sides of the foil at flow speeds, U , in ft/sec of 50, 100, and 150 with separations of $r_2(\text{SN})=0.071\text{-inch}$ and $r_2(\text{RN})=1.38\text{-inch}$	19
3.2	Power spectra of the surface pressures at 100 ft/sec at the airfoil leading edge for the round nose (RN), intermediate nose (IN), wedge nose (WN) and sharp nose (SN).....	20

3.3	Power spectra of the surface pressures at 150 ft/sec at the airfoil leading edge for the round nose (RN), intermediate nose (IN), wedge nose (WN) and sharp nose (SN).....	21
3.4	Chordwise variation of the magnitude of the surface pressure cross spectrum for a flow speed of 100 ft/sec on the sharp-nosed foil (SN) for a variety of streamwise distances (in inches) downstream of the leading edge of 0.15, 0.27, 0.47, 0.97, and 1.97	22
3.5	Chordwise variation of the surface pressure cross spectra taken near the leading edge of the sharp nose foil (SN) for various fixed frequencies	23
3.6	Surface pressure cross power spectrum magnitude and phase from measurements on opposite sides of the leading edge of the wedge nose (WN) at $U_0=100$ ft/s.....	24
3.7	Surface pressure cross power spectrum magnitude and phase from measurements on opposite sides of the round nose on the leading edge at $U_0=100$ ft/s	25
3.8	Surface pressure cross power spectrum magnitude and phase from measurements on opposite sides of the intermediate nose (IN) at the leading edge at $U_0=100$ ft/s.....	26
3.9	Surface pressure cross power spectrum magnitude and phase from measurements on the same side of the foil near the leading edge of the intermediate nose (IN) at $U_0=100$ ft/s.....	27
3.10	Cross power spectrum magnitude and phase of surface pressures from measurements on the same side of the wedge nose (WN) near the leading edge at $U_0=100$ ft/s.....	28
3.11	Lifting component of the pressure cross spectrum for the wedge nose (WN) and round nose (RN) at $U_0=100$ ft/s from measurements on opposite sides near the leading edge	29
3.12	Cross power spectrum magnitude and phase from pressures measured on opposite sides of the foil near the leading edge of the round nose (RN) and the 16 degree wedge (SN) at $U_0=50$ ft/s.....	30
3.13	Cross power spectrum magnitude and phase from pressures measured on opposite sides of the foil near the leading edge of the round nose (RN) and the 16 degree wedge (SN) at $U_0=100$ ft/s.....	31

ABSTRACT

Surface pressure cross spectral measurements near the leading edges of a variety of airfoils in a turbulent flow disclose contributions from the near fields of the diffracted pressures and the incident pressures from the grid-generated turbulence. The thickness dependence of the measured cross spectra of the near field components of the diffracted surface pressures corresponds to the thickness dependence of the dipole sound measured in the far field.

ADMINISTRATIVE INFORMATION

This work was funded in part by the Office of Naval Research 6.2 Hydroacoustics Program. The Document/Sponsor no. was N0001401WX20236, ACRN AA, the Program element no. was 0602121N, and the Project Task area is 02331. Drs. Patrick Purtel and Ki-Han Kim were the program managers. This work was also funded in part by the 93R Advanced Propulsors Program, Task 1 Blade Shaping. The Document/Sponsor no. was N0002402WR10228, the appropriation was RDT&E, the Program Element no. was 0603561N, and the Project Task no. was S2033. Mr. Doug Dahmer and Ms. Meg Stout were the program managers.

1. Introduction

The diffraction of turbulence by the leading edge of a foil produces unsteady lift and dipole sound. The dependence of the foil thickness on the dipole sound was determined from measurements by Paterson and Amiet (1976, 1977) and Olsen and Wagner (1982). These measurements demonstrated that the foil's thickness attenuates the leading edge lifting dipole sound progressively with increasing frequency over that for the zero-thickness case modeled by Sears (1941). Numerical simulations in the spatial domain using blade vortex interaction (BVI) methods by Martinez and Rudzinski (1997) and Grace (2001) have also captured the affect of foil thickness on the unsteady lift.

Gershfeld (2003) accounted for the thickness effect by modeling the dipole sound as a leading edge diffraction problem using an acoustic analogy and a shape dependent Green function [Howe (1998 a, b)]. In this analysis, the magnitude of Sears' (1941) function, $|S(k_1, h)|$, for a foil with thickness, h , was determined to be

$$|S(k_1, h)| \approx |S(k_1)| e^{-k_1 h/4}, \quad (1.1)$$

where $|S(k_1)|$ is the magnitude of Sears' (1941) function for the foil with $h=0$ and k_1 is the wave number component in the streamwise direction. When the flow with velocity, U , in the leading edge diffraction zone is assumed to be frozen in the streamwise direction, then $k_1 = \omega/U$ in Eq. (1.1) and the frequency dependence of the thickness correction is obtained. Figures (1.1) and (1.2) [Gershfeld (2003)] show respectively, a comparison of the measured dipole sound from Paterson and Amiet (1976, 1977) and the predicted dipole sound for a foil with thickness to chord, c , ratio of zero ($h/c=0$), and with a thickness to chord ratio of the NACA 0012 section, $h/c=0.12$. The thickness effect is incorporated in the near field portion of the Green function that determines, in part, the net dipole force associated with the acoustic radiation from the diffraction of turbulence by an edge of a given geometry [Howe (1998a, b)].

The acoustic analogy thickness theory is restricted to predicting the scattered pressures in the far field since this enables the near field and the far field components of Green's function to be separated. This form of Green's function cannot account for the surface distribution of the scattered pressures that determine the dipole force when the surface is not in the far field. This is especially the case in the vicinity of the leading edge region where the diffracted surface

pressures are the largest. The theories that describe the scattered surface pressure variation by Sears (1941), Osborne (1973), and Amiet (1975) are restricted to foils without thickness. These zero-thickness theories were shown by Paterson and Amiet (1976, 1977) to qualitatively describe at lower frequencies the diffracted surface pressures measured on a thick, NACA 0012 foil.

Sears' function and the thickness correction (Eq. 1.1) depend only on k_1 . Therefore, the diffracted pressures from the thick foil do not couple directly to the normalized wave number spectrum of the incident up-wash velocity, $\phi_2(k_2)$, in the thickness direction (2) except indirectly at $k_2=0$. Gershfeld (2003) has shown that the incident pressures depend on the integral length scale of the up-wash velocity component in the thickness direction, $l_2/\pi=\phi_2(k_2=0)$. The diffracted pressures must also depend on $\phi_2(k_2=0)$ since they are proportional to the incident pressures.

At high reduced frequencies, $\omega h/U$, the diffracted surface pressures are likely to be difficult to measure since the ratio of the diffracted pressure field to the incident field is substantially proportional to Eq. (1.1). This makes it likely that at high frequencies where the foil thickness reduces the magnitude of the dipole force, the incident pressures will dominate the near field components of the diffracted pressures. Minniti and Mueller (1998) measured the diffracted component of the leading edge pressures on a thin foil that encountered a time mean distortion from an upstream rotor. The phase variation with frequency of the surface pressure cross spectra measured on the same side of the foil implied a convection speed equivalent to the incident field. The magnitudes of the surface pressures away from the leading edge were above the theoretical values. Both of these observations suggest that the measured pressures may have had significant contributions from the incident field.

In the current paper, cross spectral measurements of the surface pressures near the leading edges of the foils are used to distinguish between contributions to the measured total surface pressure field from the incident surface pressures and the surface pressures due to the near field component of the diffracted pressures. Since the normalized wave number spectrum of the up-wash velocity, $\phi_2(k_2)$, does not couple directly to the diffracted pressures, it is anticipated that the cross spectrum of these pressures from measurements on opposite sides of the foil would *not* be a function of the correlation coefficient of the up-wash velocity, $\gamma_2(r_2)$, in the thickness direction, r_2 , where

$$\gamma_2(r_2) = \int_{-\infty}^{+\infty} \phi_2(k_2) e^{ik_2 r_2} dk_2 \quad (1.2)$$

Since the correlation coefficient of the incident upwash velocity, $\gamma_2(r_2)$, is spatially attenuated [Corcos (1963)] in the thickness direction,

$$\gamma_2(\omega r_2 / U) = e^{-b|\omega| r_2 / U}, \quad (1.3)$$

the corresponding pressure cross spectrum of the incident pressures will be attenuated by this factor while the cross spectrum of the diffracted pressures will not be attenuated. This will be exploited to reject the incident surface pressures especially at the high frequencies where they would be expected to dominate the diffracted pressure field while the cross spectrum of the diffracted pressures will not be attenuated by Eq. (1.3). These measurements, which, when obtained from a variety of leading edge shapes will explicitly show the thickness dependence of the net force via the near field components of the diffracted surface pressure cross spectra. Section 2 describes the experiment and the motivation for the designs of the different airfoil models and Section 3 shows the surface pressure measurements that recover the unsteady lift dependence on the airfoil shape as described by Eq. (1.1).

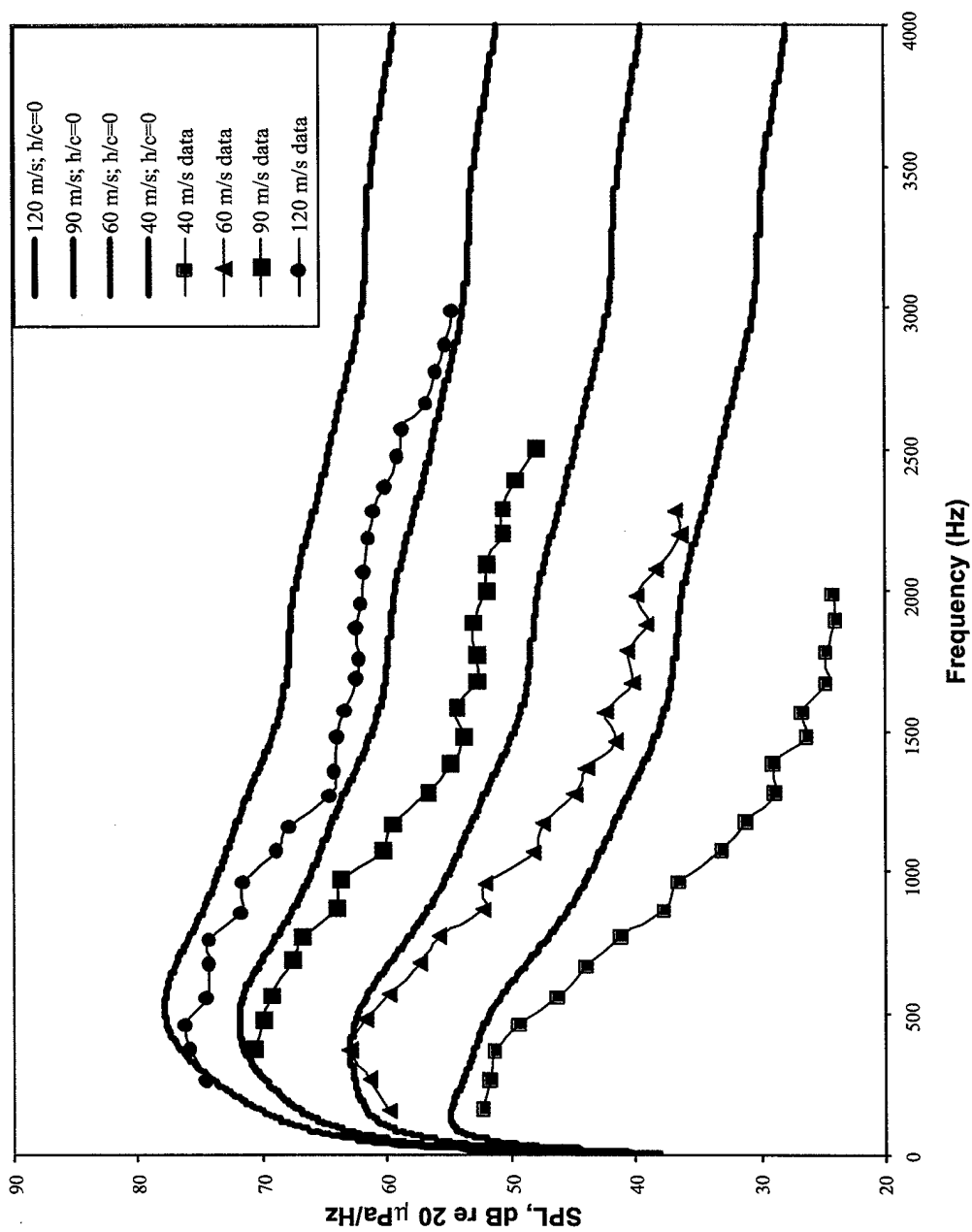


Figure 1.1. A comparison of the NACA 0012 ($h/c=0.12$) dipole sound measurements of Paterson and Amiet (1976, 1977) (points), and the thickness theory [Eq. (3.8) of Gershfeld (2003)] with $h/c=0.0$ (lines) for flow speeds of 40 m/s, 60 m/s, 90 m/s, and 120 m/s.

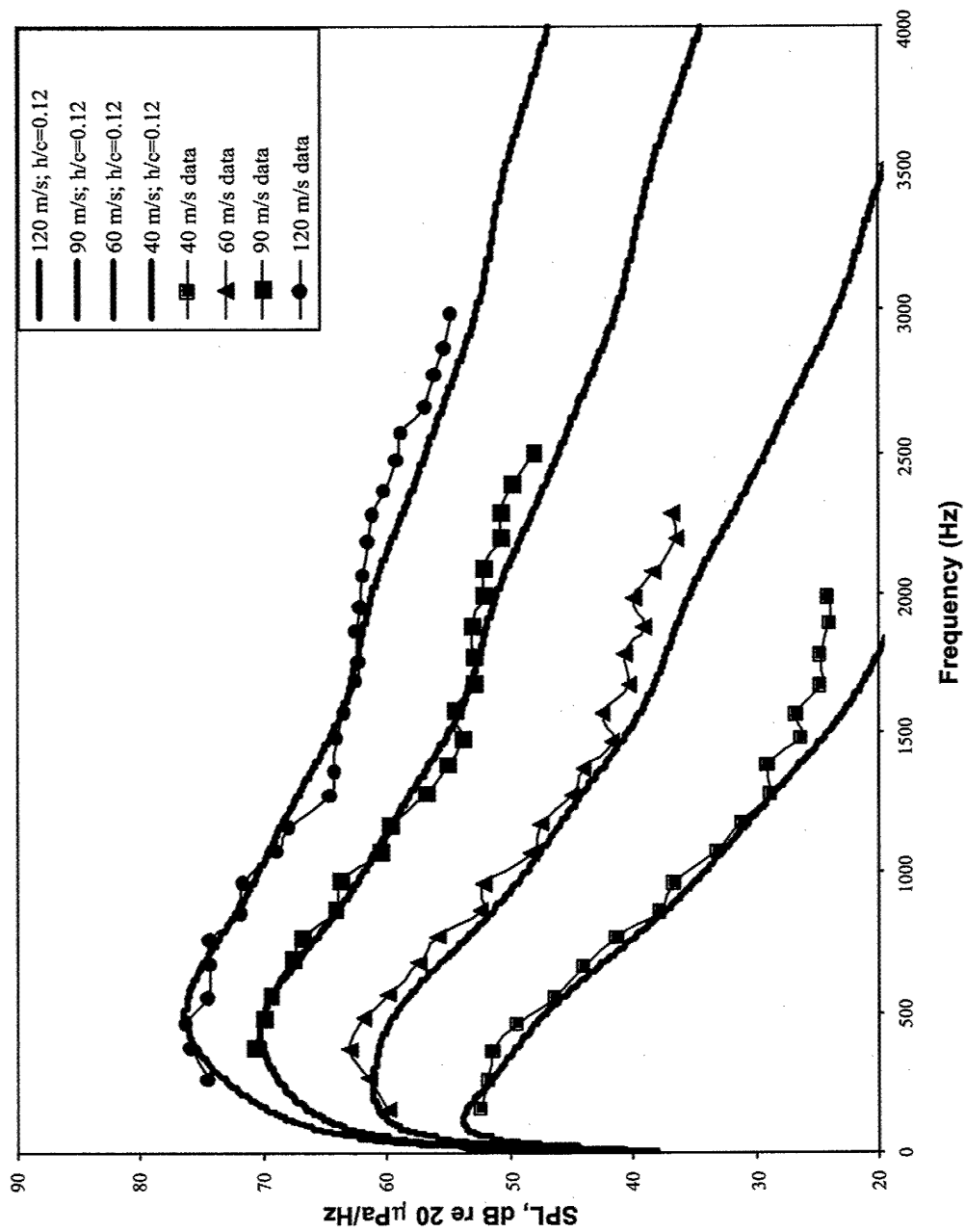


Figure 1.2. A comparison of the NACA 0012 ($h/c=0.12$) dipole sound measurements of Paterson and Amiet (1976, 1977) (points) and the thickness theory [Eq. (3.8) of Gershfeld (2003)] with $h/c=0.12$ (lines) for flow speeds of 40 m/s, 60 m/s, 90 m/s, and 120 m/s.

2. Experiment Design

Surface pressure cross spectra were measured near the leading edges of a variety of airfoils in the Anechoic Flow Facility (AFF) at NSWCCD. This facility (Fig. 2.1) houses a closed circuit, low turbulence (0.1%) wind tunnel with an 8 ft by 8 ft test section that exhausts into an anechoic room with a 23.5 ft by 23.5 ft cross section. The maximum flow speed is approximately 170 ft/s. Turbulence incident to the foil leading edge was generated by a grid located at the upstream end of the test section. The grid was composed of 4-inch diameter aluminum tubes with a center to center spacing of 1.67 ft. The tubes were bolted together at their intersections and secured to a frame that was wedged into the downstream leg of the tunnel contraction as indicated in Fig. 2.2. The 8 ft span foils were mounted at the downstream end of the test section as illustrated in Fig. 2.3. The aft 2/3 of the airfoil chord was placed in the anechoic room. A platform extended into the anechoic room and served as a support for the lower end of the foils. The upper end of the foil was secured to an angle bracket that was tied to the wall of the anechoic room by a 2-inch diameter rod. Fig. 2.4 shows a comparison of dimensionless parameters of the current design with those of Paterson and Amiet's (1976, 1977) experiment.

Data from four airfoil models are presented in this report. Figure 2.5 illustrates the dual use of a NACA 0012 airfoil with a chord length of 4 ft. In one configuration, the foil was oriented with the round nose (RN) facing upstream in order to measure the near field of the diffracted pressures associated with the foil geometry that Paterson and Amiet (1976, 1977) used to measure the dipole sound shown in Figs. 1.1 and 1.2. The second orientation placed the trailing edge of the NACA 0012 foil into the wind. This sharp nose (SN) configuration (Fig. 2.5) was used to simulate a semi-infinite wedge with a 16 deg. interior angle. When the chordwise extent of the bevel (3 ft) is much greater than the convection wavelengths, U/f , of the incident field, the length of the bevel behaves as if it were semi-infinite [Howe (1988)]. Crighton and Leppington (1975) showed that for exterior angles, α (in radians), the dipole sound power spectrum (PS) from a semi-infinite wedge can be expressed in terms of the dipole sound PS from a half-plane,

$$\Phi_{\text{wedge}}^{\text{rad}}(\omega) \approx \Phi_{1/2\text{plane}}^{\text{rad}}(\omega) \left(\frac{\omega \delta}{U} M \right)^{2\pi/\alpha - 1}, \quad (2.1)$$

where δ is the boundary layer thickness and M is the flow Mach number. The 16 deg. wedge has an exterior angle of 6 rad. The exponent in Eq. (2.1) becomes 0.04. Thus, the 16 deg. wedge (SN) has the same scattering efficiency as the half plane for all of the frequencies and flow speeds of this experiment. The sharp nose (SN) configuration permitted the near field dipole pressures to be measured for the theoretical zero-thickness case plotted in Figs. 1.1 and 1.2. A second, NACA 0018 foil was also oriented in the SN configuration with the trailing edge pointing into the flow. This foil has virtually the same scattering efficiency as the NACA 0012 foil. However, it had a metal trailing edge that allowed easier placement of the surface pressure transducers.

A third leading edge shape consisted of a local 60 deg. interior angle bevel, designated the wedge nose (WN) as illustrated in Fig. 2.6. It is shown in comparison to the RN edge configuration. The NACA 0012 foil was constructed in two parts. These parts allowed for a variety of leading edges to be bolted on to a baseline foil, forming a contiguous section shape. The baseline leading edges were formed as one-foot chord length appendages to the aft 3 ft. chord length baseline NACA 0012 section. The parting line for the fore and aft section shapes can be seen in Fig. 2.3. A fourth leading edge shape, designated as the intermediate nose (IN) was similar to the wedge edge (WN) except that the apex of the wedge was rounded with a one-half inch radius of curvature.

Surface pressures were measured with Entran EPE-C01-2P-M09F (flat) sensors and Endevco 8501C sensors. The transducers were signal conditioned by Endevco 106 amplifiers. The pressure signals were spectrum analyzed with a Hewlett-Packard 3567A analyzer. The ensemble size of the surface pressure spectra was 1,000.

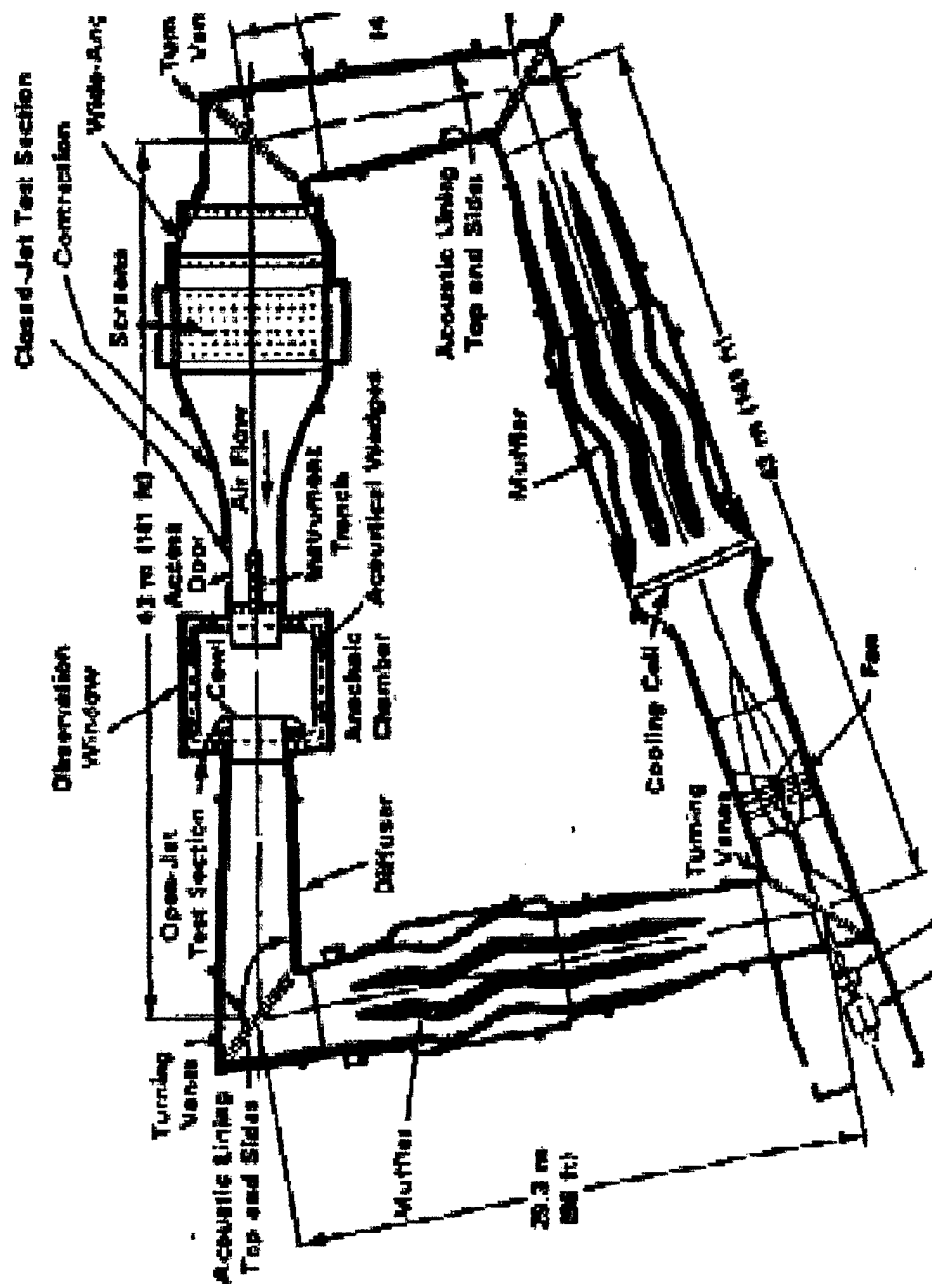


Fig. 2.1. Anechoic Flow Facility, NSWCCD.

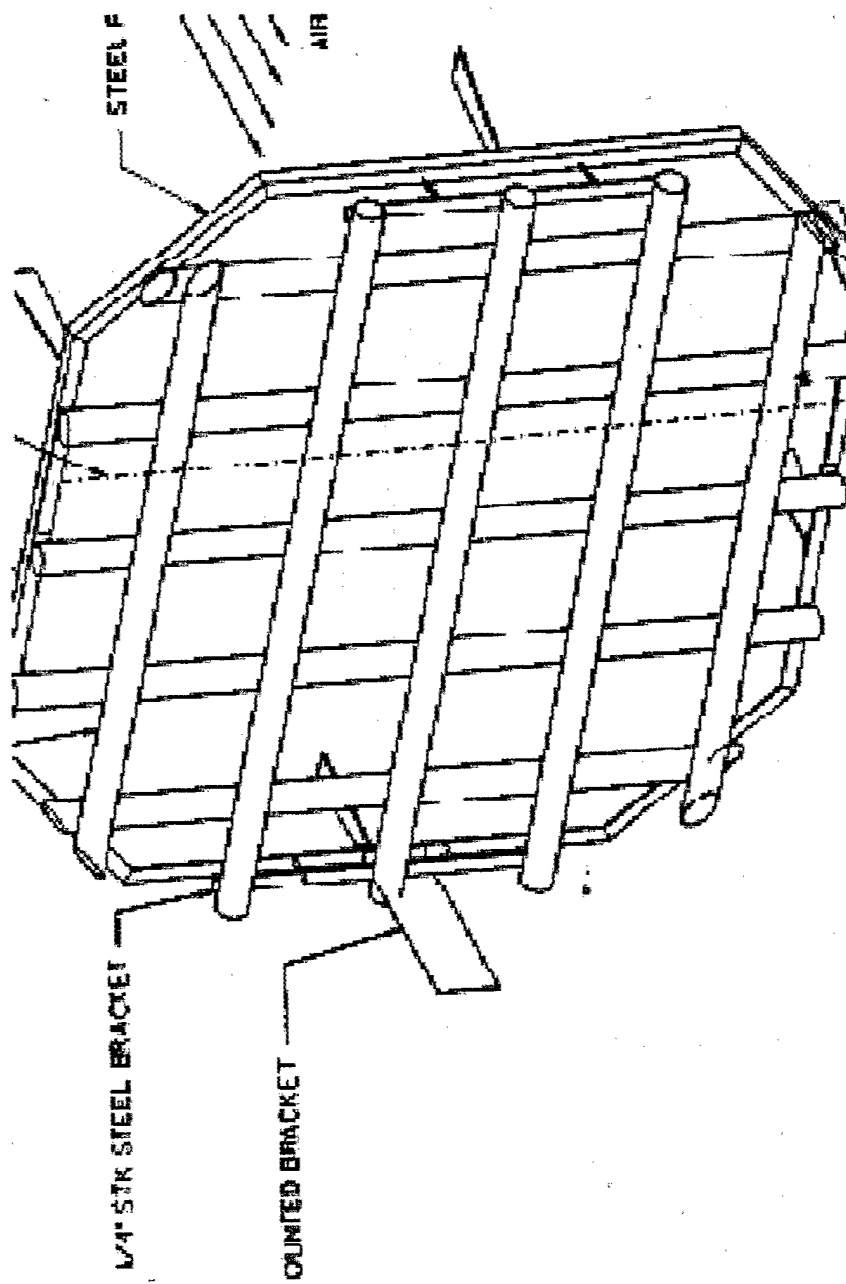


Fig. 2.2. An illustration of the turbulence generating bi-plane grid design.



Figure 2.3. Experimental configuration of turbulence generating grid and airfoil in the Anechoic Flow Facility.

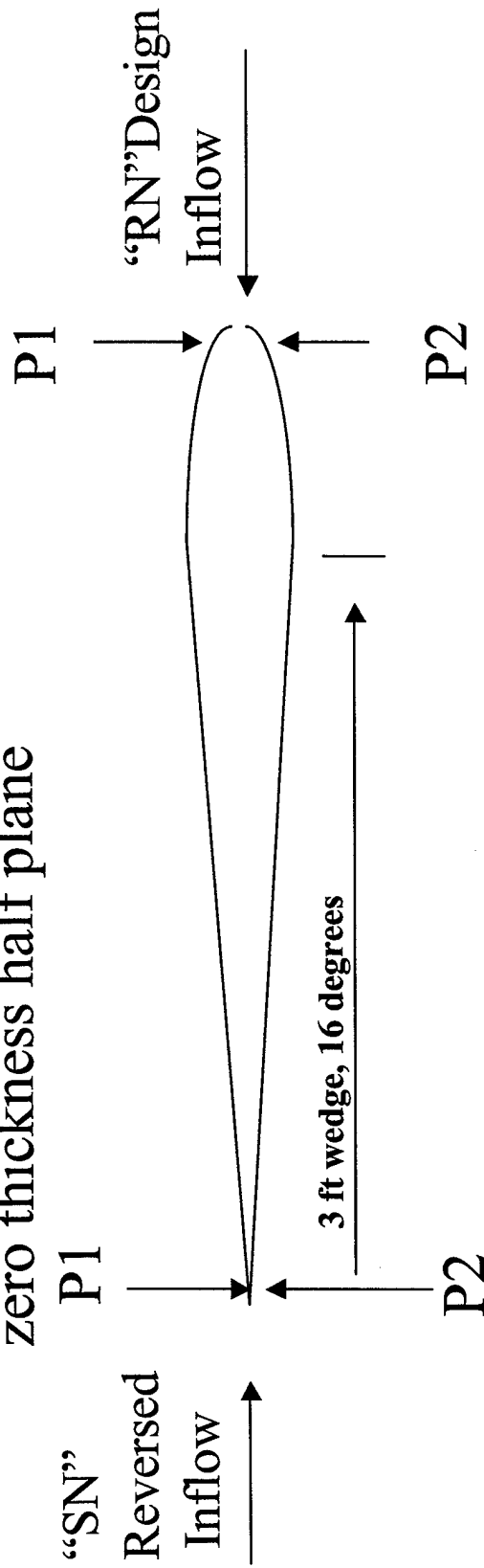
<u>Current Experiment</u>	<u>Paterson and Amiet(1976)</u>
• Rod spacing/ Rod diam = 5.0	• Rod spacing/ Rod diam = 5.25
• Foil chord/ Rod spacing = 2.4	• Foil chord/ Rod spacing = 1.73
• Distance between grid and foil/rod spacing = (9.6 - 13.2)	• Distance between grid and foil/rod spacing = (11.7)
• Reynolds number (rod diameter) (100,000- 300,000)	• Reynolds number (rod diameter) (50,000 - 200,000)

Figure 2.4. A comparison of dimensionless parameters of Paterson and Amiet (1976) and the current experiment.

“Reversed” NACA 0012 Foil:

*Simulates 16 deg.

Semi-infinite wedge ~
zero thickness half plane



Design NACA 0012 Foil: *Thick Leading Edge

Figure 2.5. Schematic of a NACA foil section shape oriented with the leading edge or round nose (RN) facing the wind and with the trailing edge or sharp nose (SN) facing the wind.

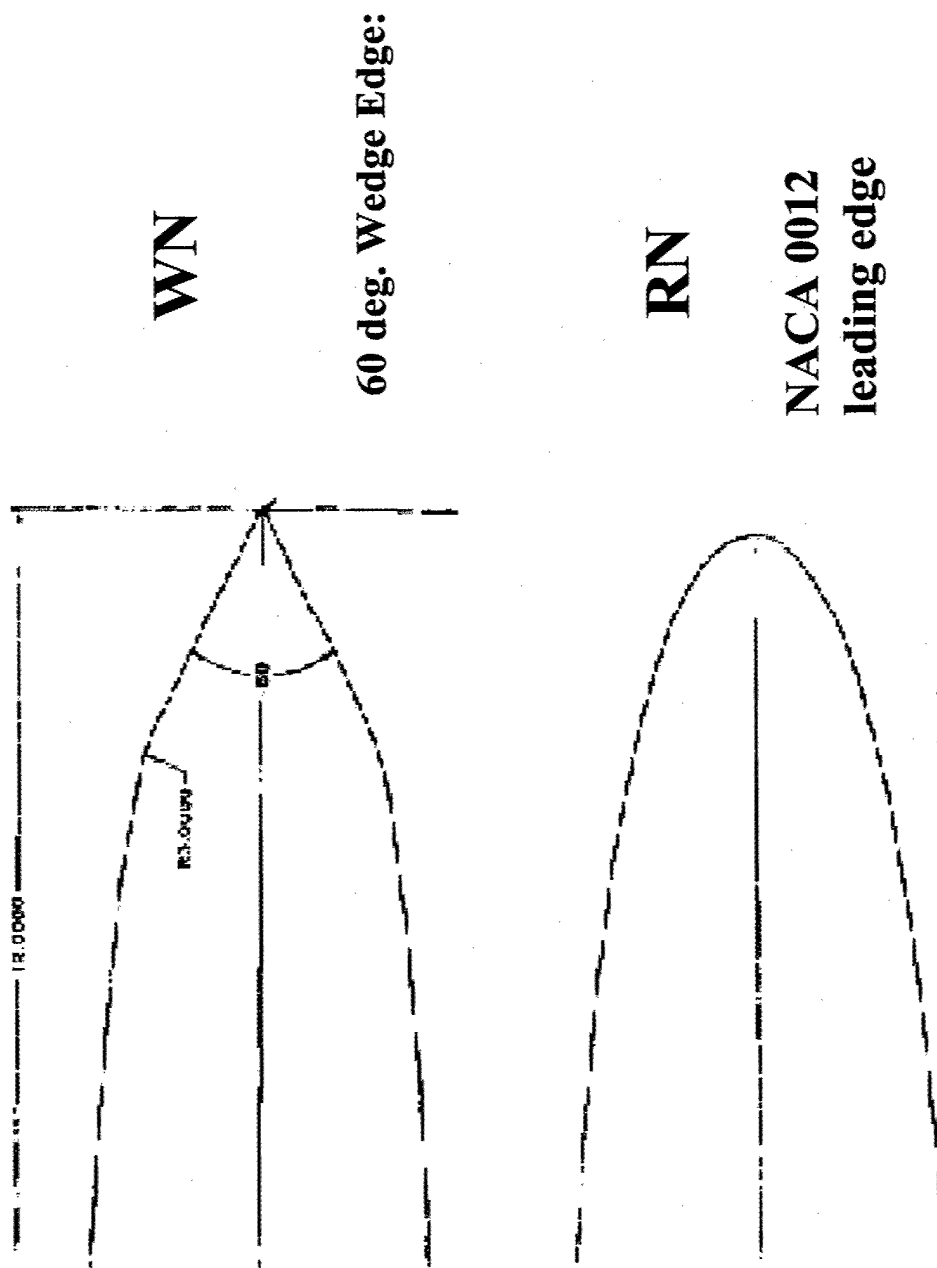


Figure 2.6. Illustrations of the wedge nose (WN) and round nose (RN) geometry.

3. Experimental Results

In this section, the magnitudes and phases of the surface pressure cross spectra measured near the leading edges of the foils described in Section 2 are presented to elucidate the distinct properties of the incident and scattered pressure fields that make up the total pressure field. The cross spectral measurements taken on opposite sides of a foil will be used to recover the “thickness effect” of the near field lifting pressures of the leading edge dipoles from the NACA0012 foil (RN) and the “zero-thickness” foil (SN) and two intermediate leading edge shapes. As discussed in Section 1, the incident surface pressure cross spectra measured on opposite sides of the leading edge are postulated to depend on the correlation coefficient in the thickness direction while the cross spectra of the scattered surface pressures do not. This will be exploited in this section to obtain the scattered pressure field at high frequencies where the thickness effect is pronounced (Fig. 1.1) and the power spectrum of the incident surface pressures is most likely to dominate the scattered pressures.

Coherence measurements, $\gamma_2(\omega r_2/U)$, of the surface pressures were obtained from surface pressure sensors located on opposite sides of the foil at a fixed streamwise position, y_1 , approximately 0.5-inch from the leading edge stagnation point. They are plotted in Fig. 3.1 for the sharp nosed foil (SN) in blue and the round nosed foil (RN) in red for flow speeds (in ft/s) of 50, 100, and 150. The sensor separation distances through the thickness of the foils, r_2 , for the SN and RN foils are 0.071-inch and 1.38-inch respectively. If the scattered field was proportional to the correlation coefficient, γ_2 of the incident field in the thickness direction,

$$\gamma_2(\omega r_2/U) = e^{-b\omega|r_2|/U}, \quad (3.1)$$

then the frequency normalization of the coherence plots in Fig. 3.1 would have normalized this dependence and only the thickness dependence of the scattered pressure field would remain. It is clear from this data that the cross spectra of the lifting pressures are independent of this correlation coefficient.

Power spectra in the leading edge region of the round nose (RN), intermediate nose (IN), wedge nose (WN), and sharp nose (SN) foils are plotted in Figs. 3.2 and 3.3 for a flow speeds of 100 ft/s and 150 ft/s respectively. The power spectra do not exhibit the thickness dependence in

the high frequencies as do the dipole sound predictions as illustrated in Figs. 1.1 and 1.2. In the high frequencies, it will be shown that the power spectra are dominated by the incident pressures associated with the near field component of the quadrupole radiation from the grid generated turbulence.

Figure 3.4 illustrates the chordwise variation of the magnitudes of cross spectra taken at 100 ft/s with sensors on opposite sides of the sharp nose foil (SN) foil for distances from the leading edge in inches of 0.15, 0.27, 0.47, 0.97, and 1.97. These data are plotted for fixed frequencies as a function of distance away from the leading edge in Fig. 3.5. The chordwise variation is compared with the theoretical variation that reduces as the inverse of the distance away from the leading edge. At low frequencies, the pressure power spectra reduce as the reciprocal of the distance from the leading edge. This compares favorably to the zero-thickness theory [Sears (1941)]. The reduction in pressure level as a function of chordwise distance from the leading edge is broadband in frequency. This suggests that the cross spectrum measurement is dominated by the scattered pressure field and that the incident pressure field is rejected.

Figure 3.6 illustrates the magnitude and phase of the cross spectrum of the pressure field measured at 100 ft/s near the leading edge of the wedge nose (WN) foil. The pressure sensors were located on opposite sides of the foil and at the same streamwise location, $y_1=0.5$ in., relative to the leading edge. Below 800 Hz, the phase difference between the upper and lower surfaces is π and the amplitude is reducing relatively quickly in frequency in accordance with the scattered field being proportional to "Sears' function." These properties are indicative of the near field pressures associated with the leading edge dipoles due to the diffracted turbulence by the leading edge. Above 800 Hz, the phase difference is zero between the pressures on opposite sides of the foil. This is indicative of the incident pressure field which sees no variation in the convection phase, $\omega r_1/U$, with frequency when the streamwise separation between the sensors is zero ($r_1=0$). This is in accordance with Corcos' (1963) representation of the wall pressure cross spectrum:

$$\Phi_{pp}(r_1, r_3, \omega) = \Phi_{pp}(\omega) e^{-a\omega|r_1|/U} e^{i\omega r_1/U} e^{-\beta\omega|r_3|/U} \quad (3.2)$$

The streamwise separations are a function of r_1 and have a phase variation with frequency. The components without a streamwise separation (either in the spanwise direction of the foil or through the thickness of the foil) have no phase variation with frequency.

Figure 3.7 shows the same measurement as Fig. 3.6 for the round nose foil, (RN). This plot suggests that the unsteady lifting pressures generated by the round nose are weaker than those created by the wedge nose. The magnitude and the phase of the cross spectrum shows the same behavior as the other edge illustrated in Fig. 3.6. Below 600 Hz, the pressure field is dominated by the near field pressures of the diffracted field. Above 600 Hz, the pressures are dominated by the incident pressure field. The streamwise transducer separation distance is zero ($r_1 = 0$), and the incident pressures are in phase. Since the incident pressure field is the same for both measurements, the unsteady lifting pressures dominate the incident pressure field up to a lower maximum frequency of 600 Hz for the round nose (RN) while the wedge nose (WN) dominates the incident field up to 800 Hz.

Figure 3.8 illustrates a cross spectrum of the surface pressures near the leading edge of the intermediate nose (IN). The sensors were located on opposite sides of the foil near the leading edge. Below 600 Hz, the total pressure field is dominated by the lifting pressures associated with the dipoles and the phase difference is 180 deg. At higher frequencies, the magnitude of the cross spectrum is similar to those presented in Figs. 3.6 and 3.7. However, the phase difference is not 0 deg.

The pressures of the leading edge dipoles are 180 deg. out of phase for positions on opposite sides of the foil near the leading edge. The dipole pressures are in phase for pressures on the same side of the foil. Surface pressure cross spectra measured near the leading edge of the foil but on the same side should have pressures that are in phase in the lower frequencies where the scattered field should dominate the total pressure field. As described by Eq. (3.2), the incident pressure field phase will vary as $\omega r_1 / U$ for surface pressure cross spectra obtained with sensors that are displaced a streamwise distance, r_1 . Figure 3.9 shows the magnitude and phase of the cross spectrum of surface pressures measured near the leading edge of the intermediate nose (IN) on the same side of the foil with a streamwise sensor displacement of $r_1 = 1$ -inch. Below 400 Hz, the total pressure field is dominated by the dipole pressures as suggested by the frequency dependence of the magnitude of the cross spectrum and the phase. Above 400 Hz, the phase varies in accordance with convection speed of 100 ft/s and a sensor separation of distance of 1-inch. This indicates that above 400 Hz, the surface pressure field is dominated by the incident pressures from the near field of the quadrupole pressures of the grid generated turbulence.

Figure 3.10 shows the magnitude and phase of the surface pressure cross spectrum for pressures measured on the same side of the foil near the leading edge of the wedge nose foil (WN) for a flow speed of 100 ft/s. Below 400 Hz, the pressures are in phase in accordance with the dipole lifting pressures and above this frequency, the total surface pressure field is dominated by the incident field with a phase variation of a convecting pressure field.

The magnitudes of the pressure cross spectra taken on opposite sides of the foil near the leading edge are a metric of the magnitude of the unsteady lift generated by the leading edge dipoles. In Fig. 3.11, the magnitudes of the cross spectra from surface pressure measurements made on opposite sides of the wedge nose (WN) and the round nose (RN) foils are plotted. The round nose has a slightly reduced spectral level for increasing frequencies than the wedge nose. Even though the wedge nose has a leading edge that approaches a zero radius of curvature, the chordwise extent of the bevel of the wedge is not sufficiently large enough to simulate the scattering efficiency of the semi-infinite wedge.

The sharp nose (SN) and the round nose (RN) cross spectra are plotted in Figs. 3.12 and 3.13 for flow speeds of 50 ft/s and 100 ft/s. These plots show respectively, the relative exponential reduction in scattered surface pressure cross spectra for the round nose relative to the sharp nose configurations. The relative difference in the unsteady lift cross spectra corresponds to the theoretical result of the thickness correction to Sears' (1941) function [Gershfeld (2003)] as indicated in Eq. (1.1) for frequencies less than 400- 500 Hz. Above this frequency range, the incident pressures dominate the pressure spectra for the RN configuration. The sharp nose foil appears to have a sufficiently long chordwise extent of a bevel to simulate the scattering efficiency of the semi-infinite wedge. Included in these figures are the phases of the cross spectra of the SN foils showing the 180 deg phase difference due to the lifting pressures.

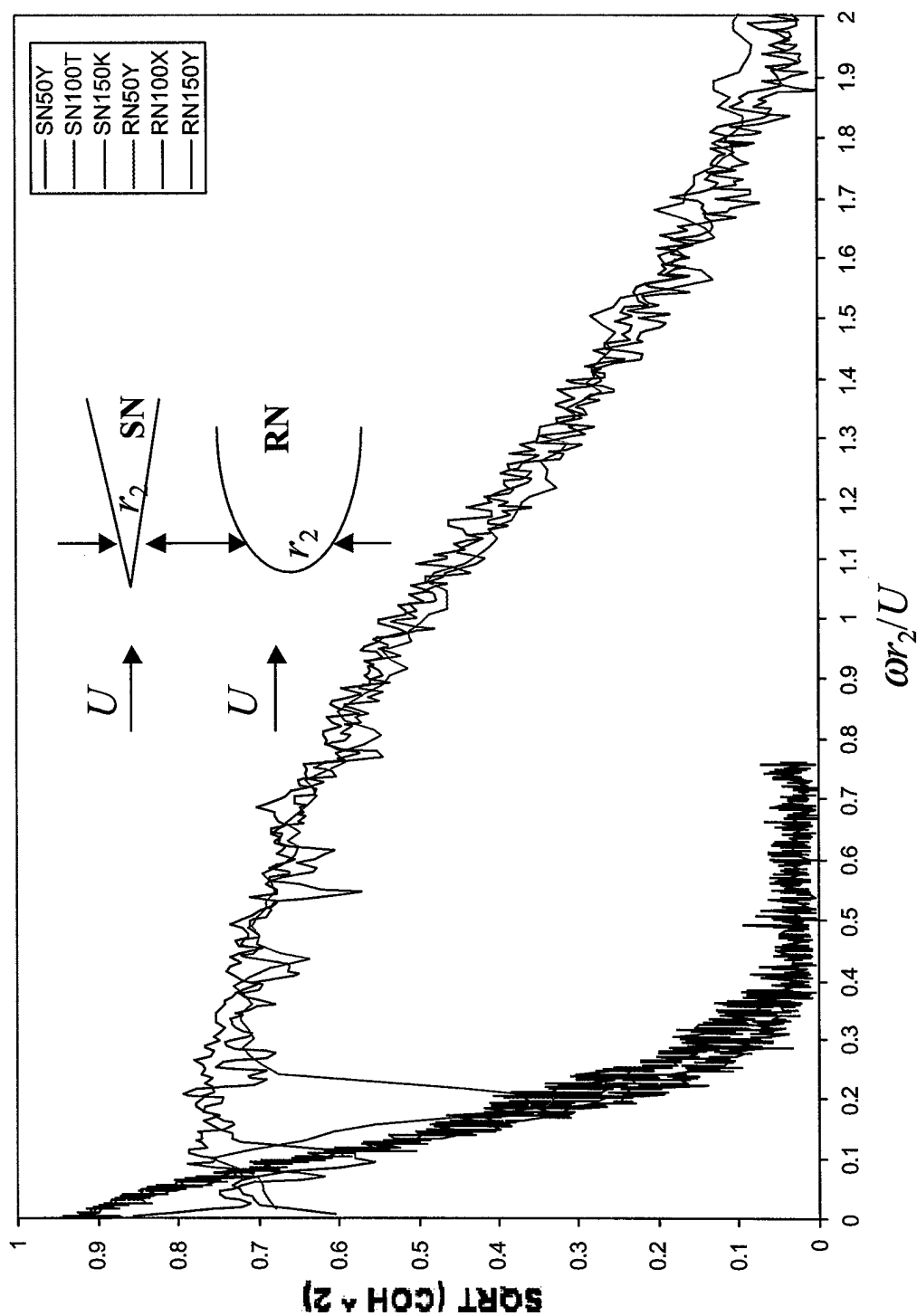


Figure 3.1. Coherence functions, $\gamma(\omega_r/U)$ for sharp nose (SN), and round nose (RN) leading edges obtained from surface pressures measured on opposite sides of the foil at flow speeds, U , in ft/sec of 50, 100, and 150 with separations of r_2 (SN)=0.071-inch and r_2 (RN)=1.38-inch

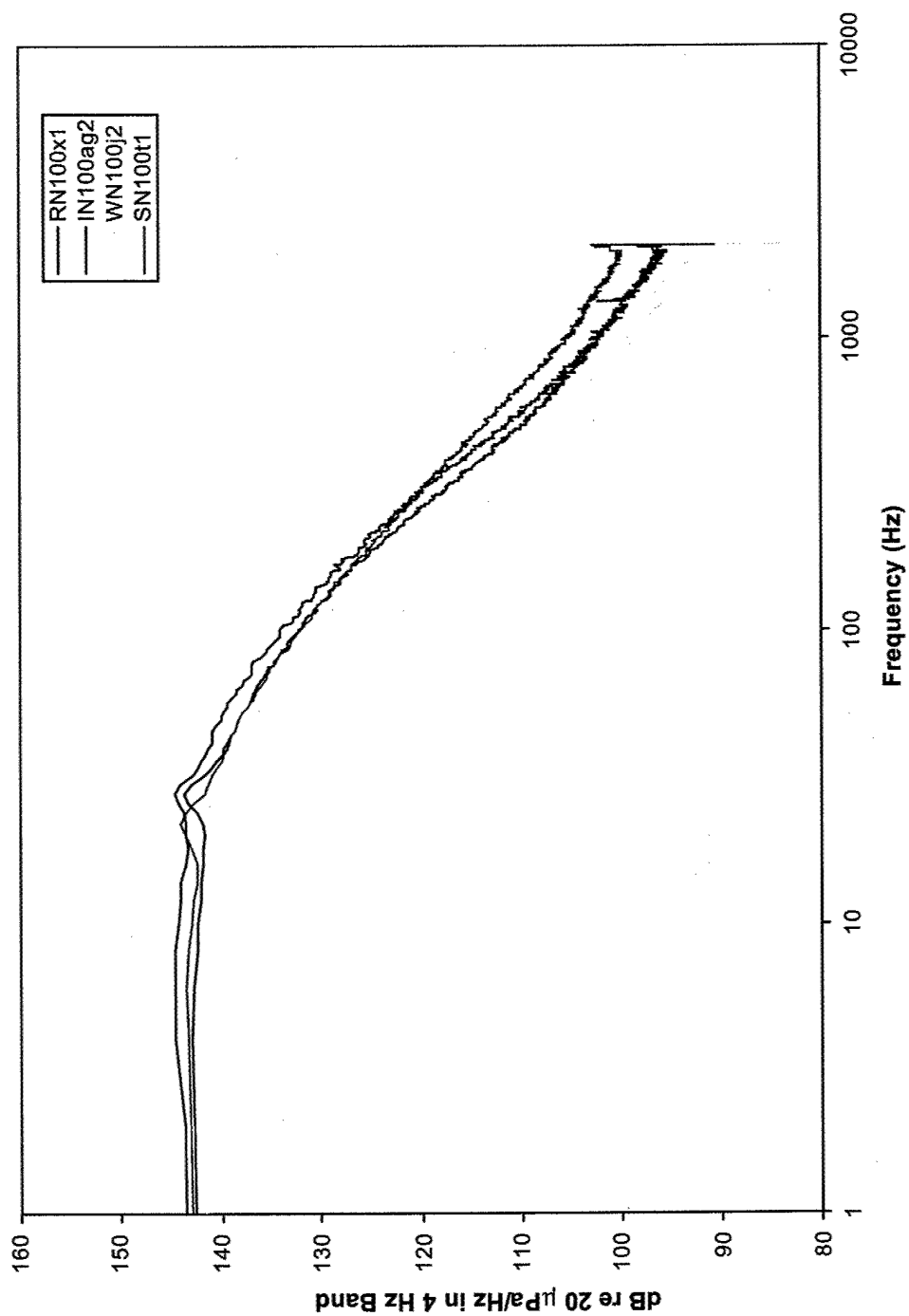


Figure 3.2. Power spectra of the surface pressures at 100 ft/sec at the airfoil leading edge for the round nose (RN), intermediate noise (IN), wedge nose (WN), and sharp nose (SN).

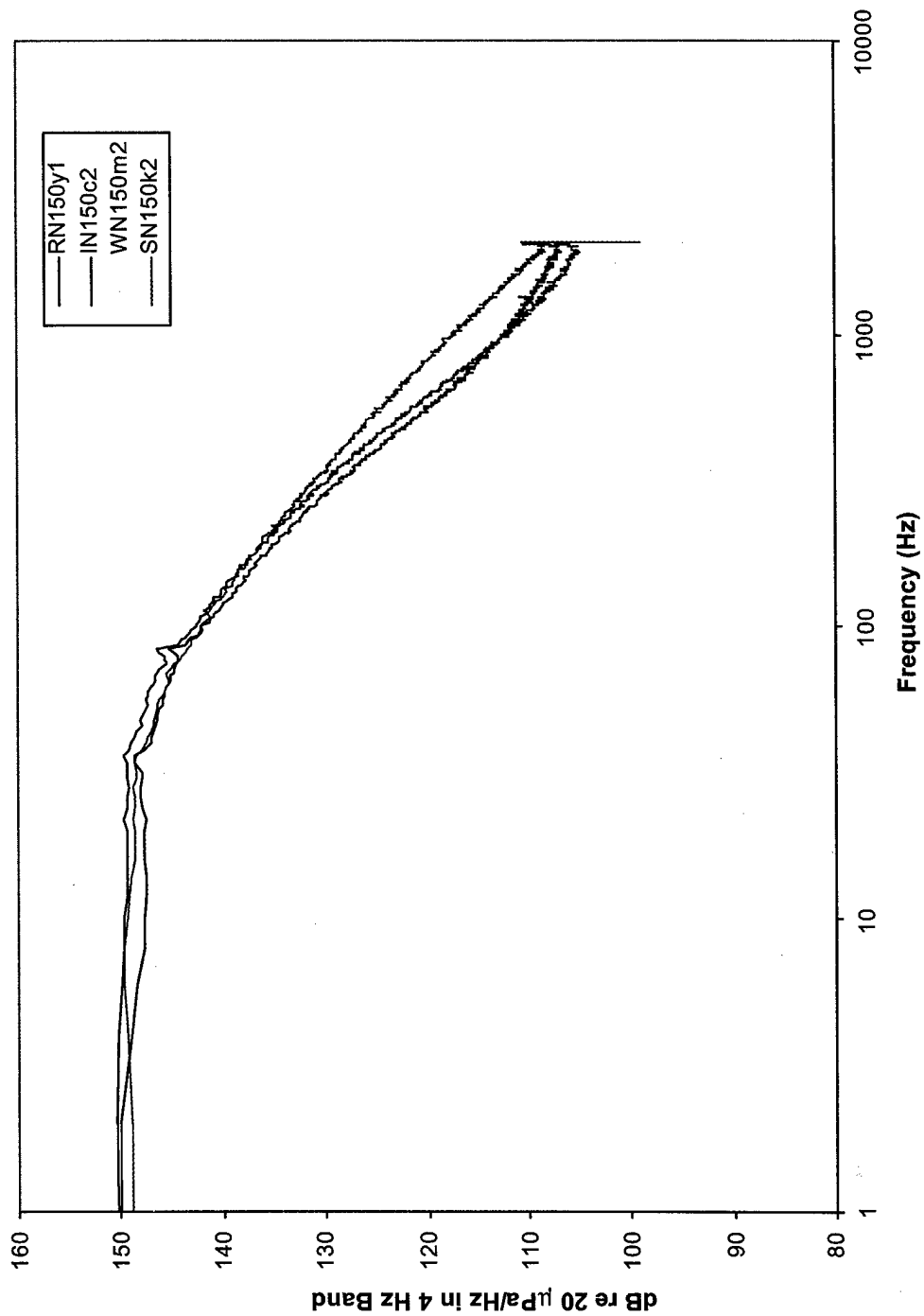


Figure 3.3. Power spectra of the surface pressures at 150 ft/sec at the airfoil leading edge for the round nose (RN), intermediate nose (IN), wedge nose (WN), and sharp nose (SN).

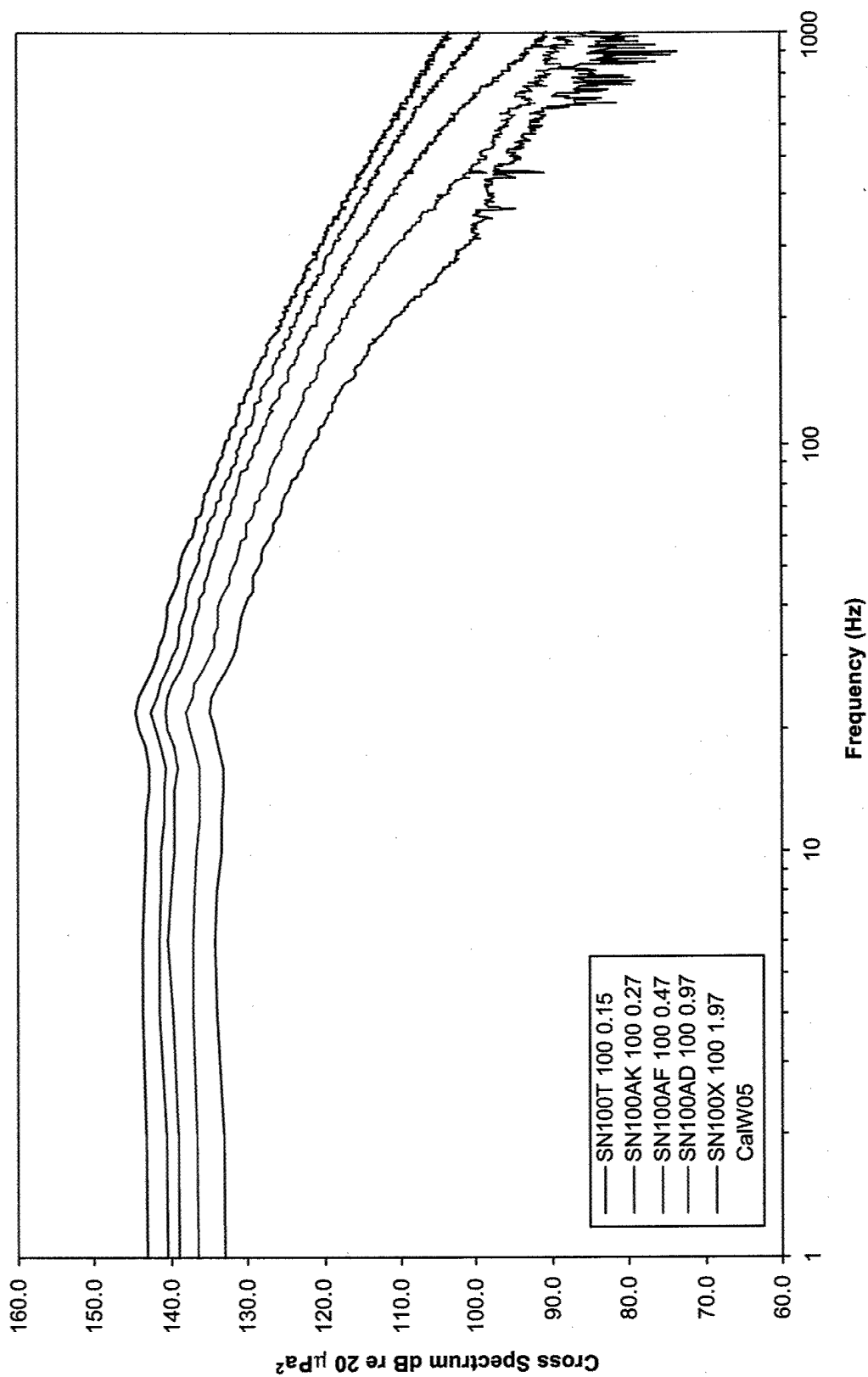


Figure 3.4. Chordwise variation of the magnitude of the surface pressure cross spectrum for a flow speed of 100 ft/sec on the sharp-nosed foil (SN) for a variety of streamwise distances (in inches) downstream of the leading edge of 0.15, 0.27, 0.47, 0.97, and 1.97.

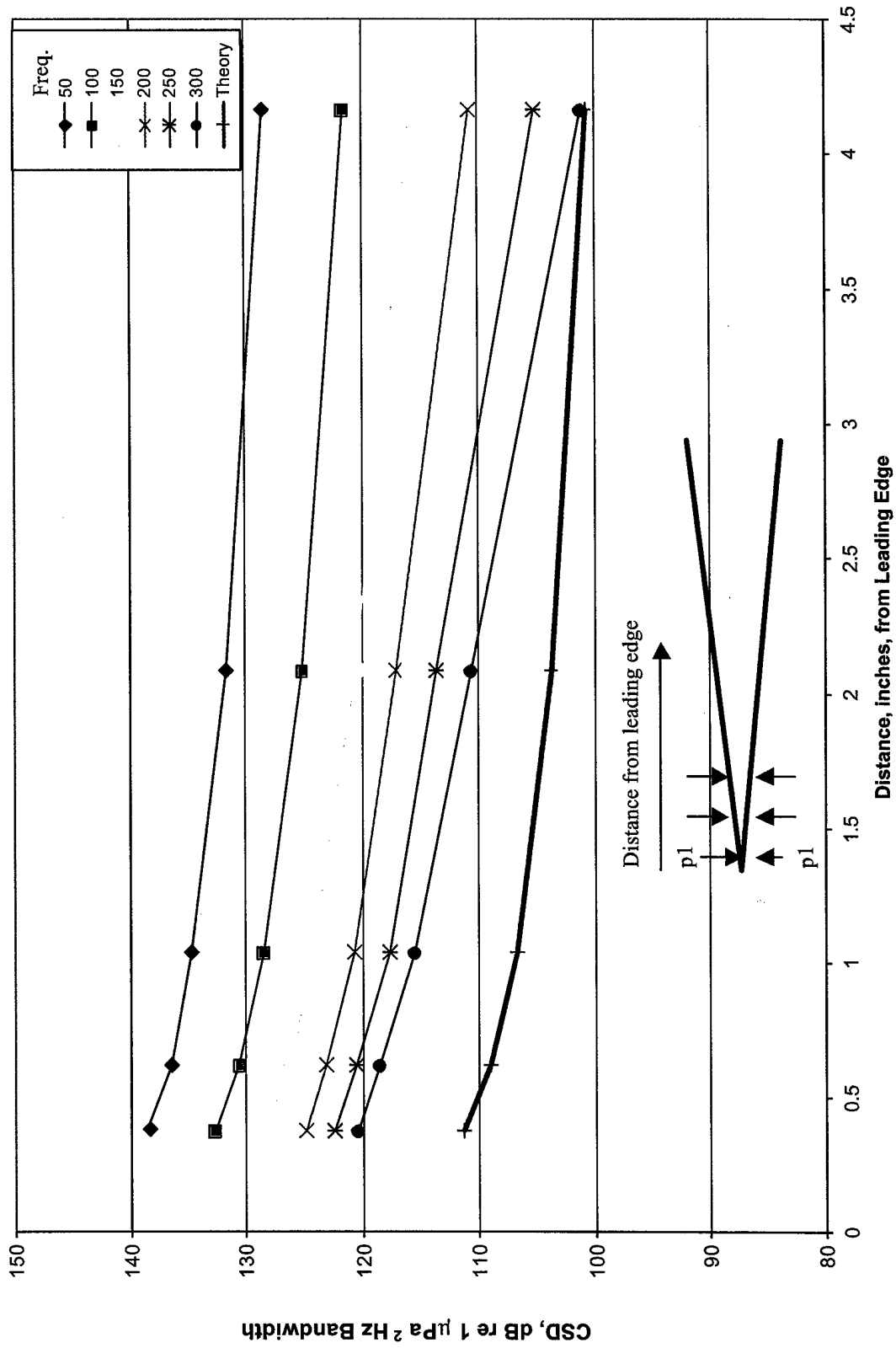


Figure 3.5. Chordwise variation of the surface pressure cross spectra taken near the leading edge of the sharp nose foil (SN) for various fixed frequencies.

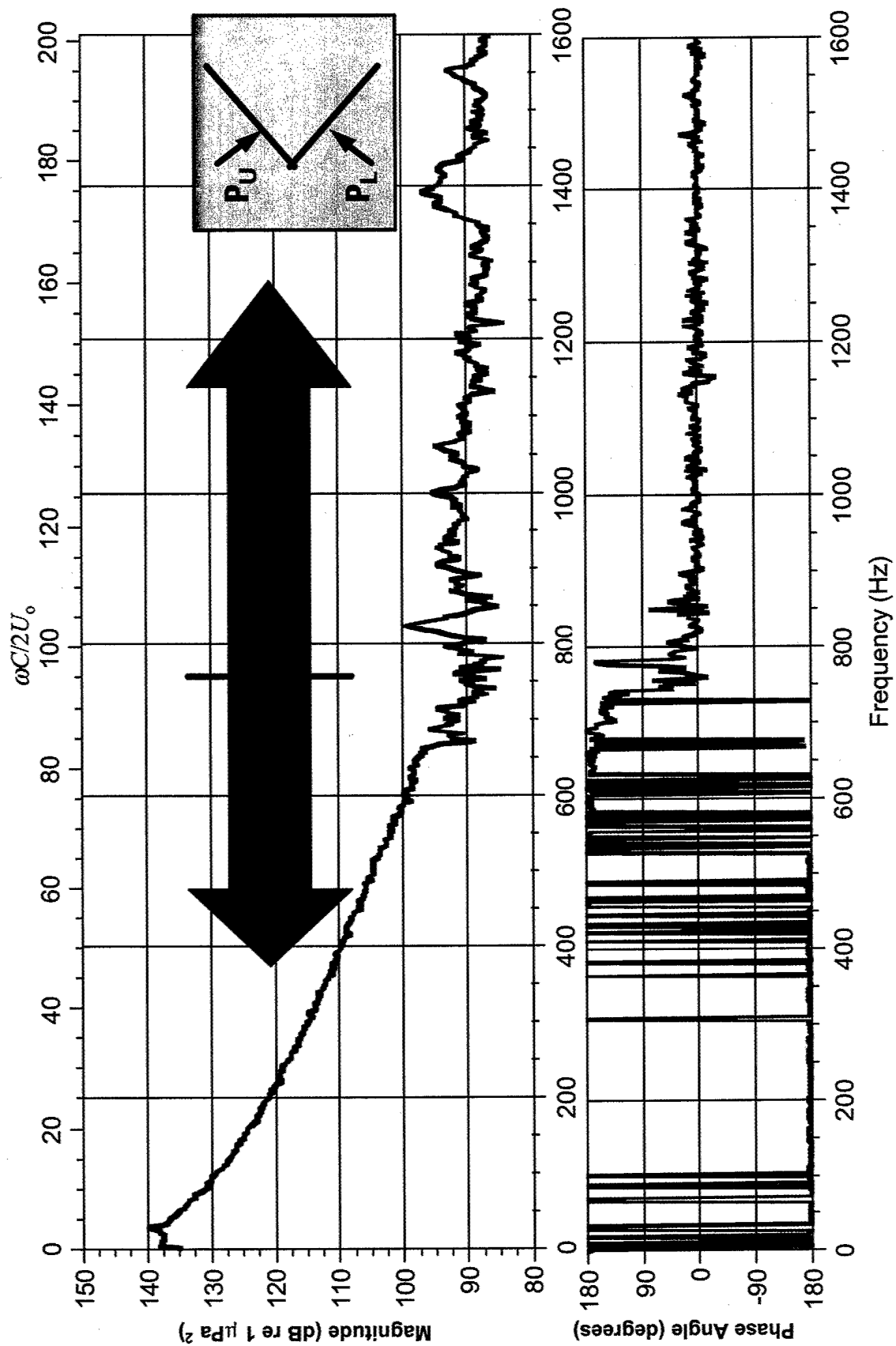


Figure. 3.6. Surface pressure cross power spectrum magnitude and phase from measurements on opposite sides of the leading edge of the wedge nose (WN) at $U_0 = 100$ ft/s.

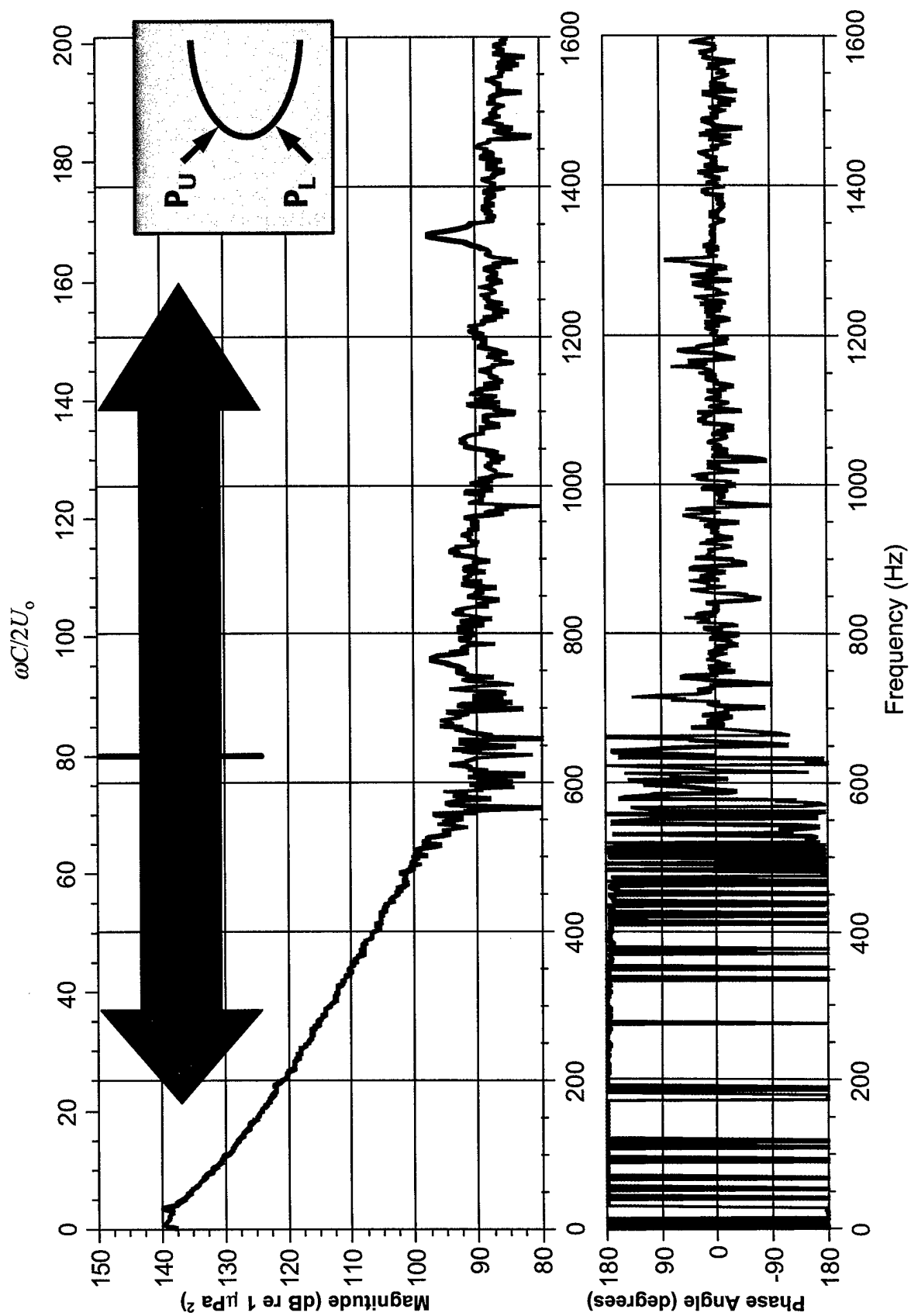


Figure 3.7. Surface pressure cross power spectrum magnitude and phase from measurements on opposite sides of the round nose (RN) on the leading edge at $U_o = 100$ ft/s.

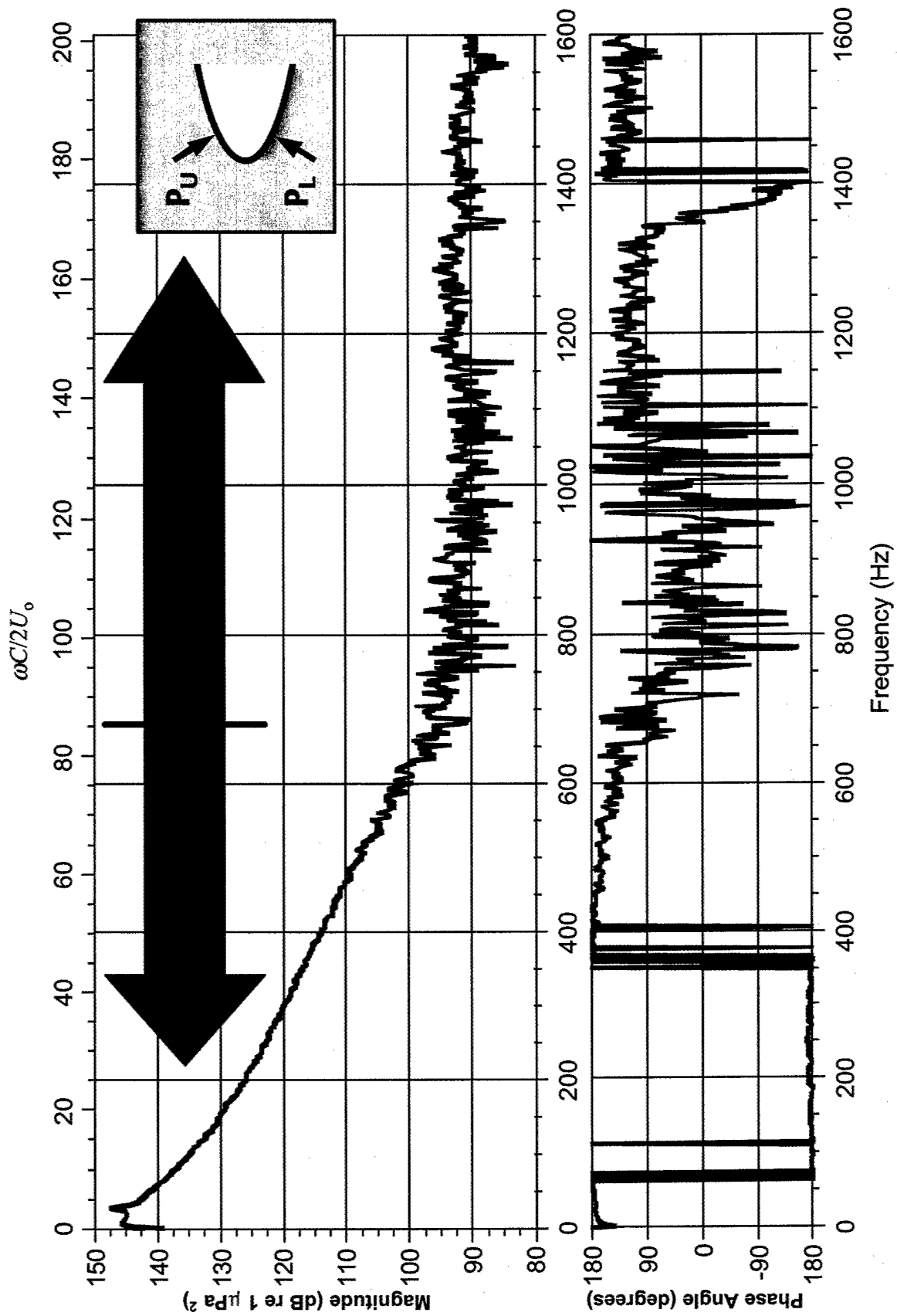


Figure 3.8. Surface pressure cross power spectrum magnitude and phase from measurements on opposite sides of the intermediate nose (IN) at the leading edge at $U_o = 100$ ft/s.

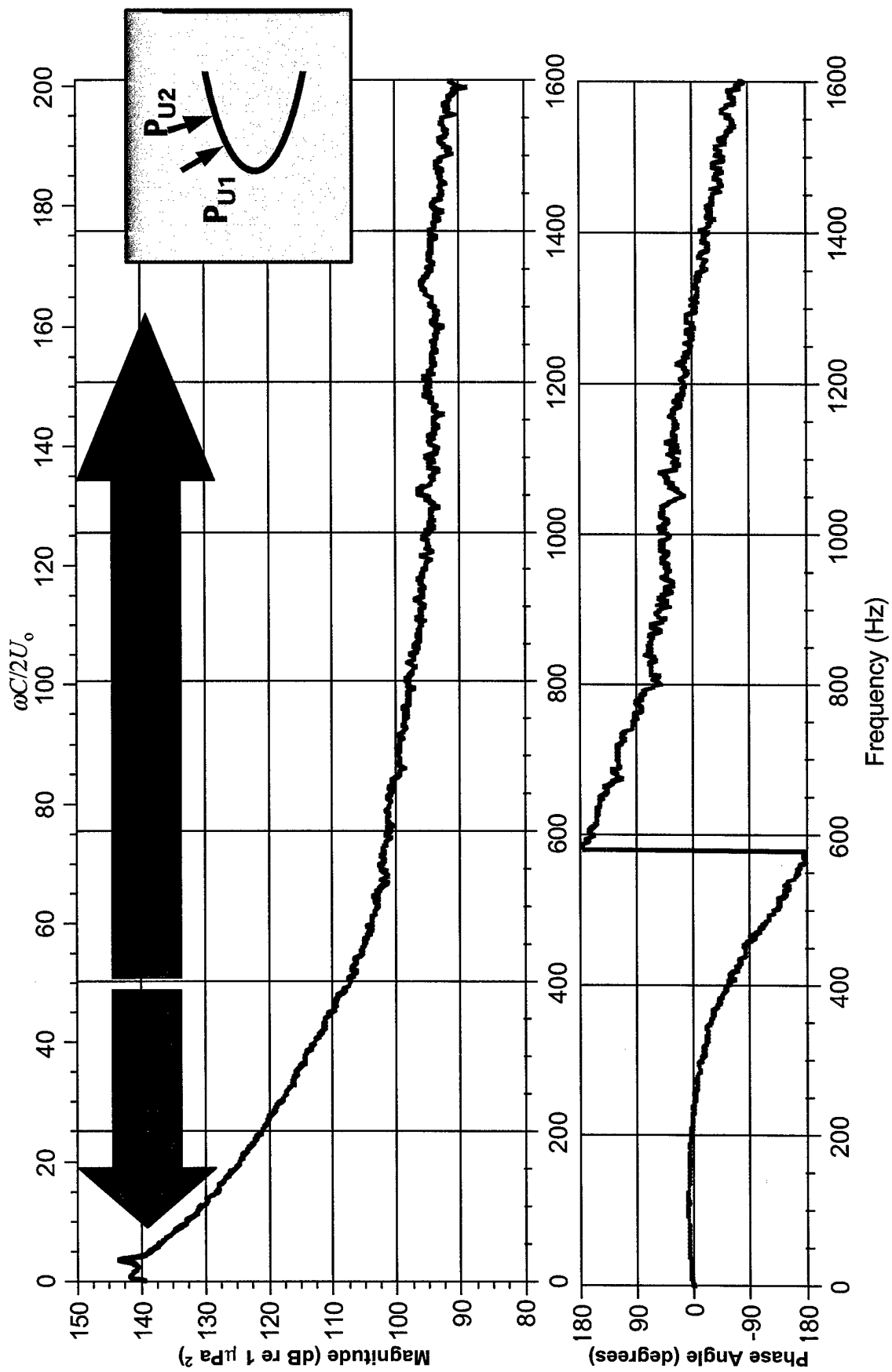


Figure 3.9. Surface pressure cross power spectrum magnitude and phase from measurements on the same side of the foil near the leading edge of the intermediate nose (IN) at $U_o = 100$ ft/s.

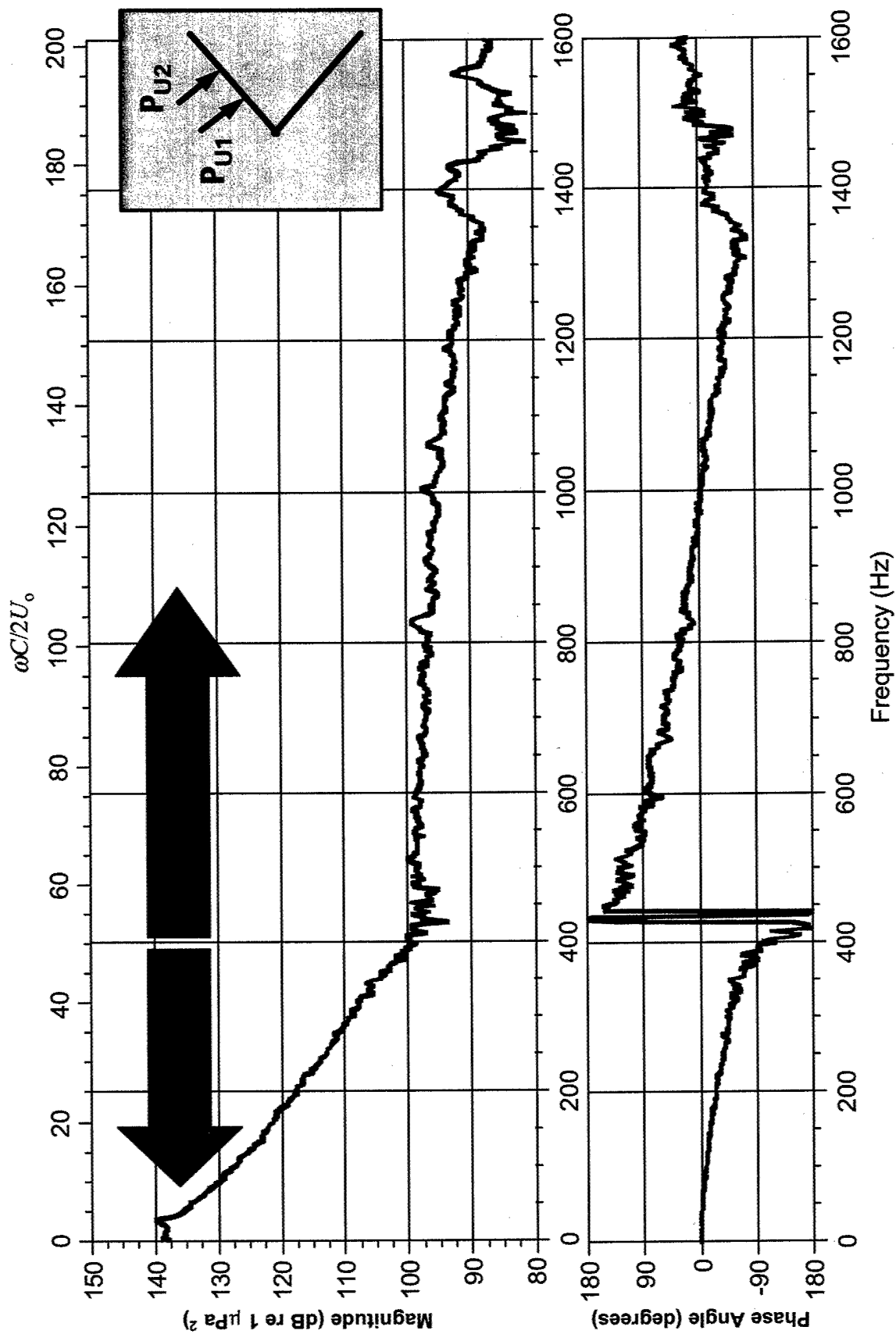


Figure 3.10. Cross power spectrum magnitude and phase of surface pressures from measurements on the same side of the wedge nose (WN) near the leading edge at $U_0 = 100$ ft/s.

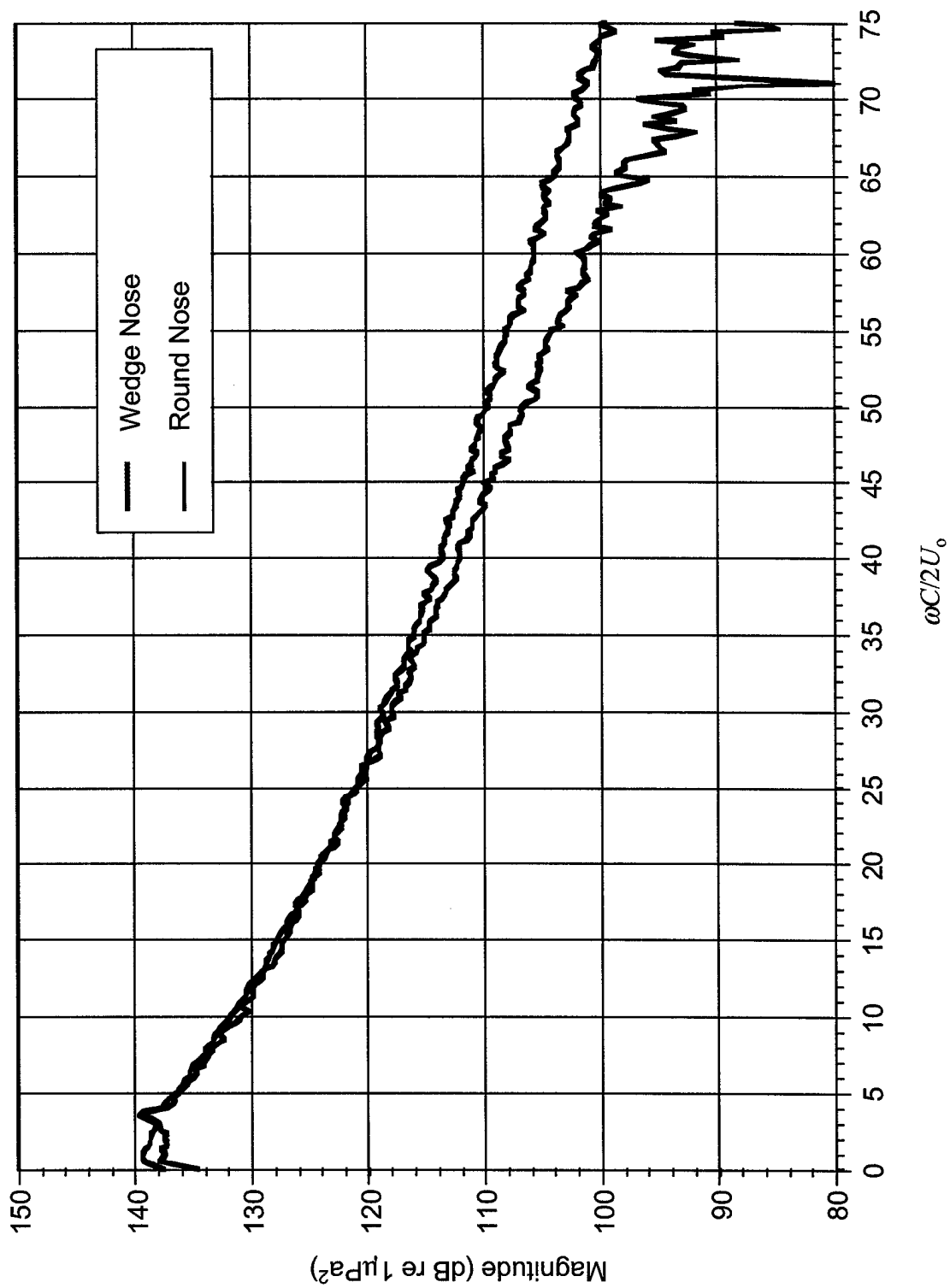


Figure 3.11. Lifting component of the pressure cross spectrum for the wedge nose (WN) and round nose (RN) at $U_0 = 100$ ft/s from measurements on opposite sides near the leading edge.

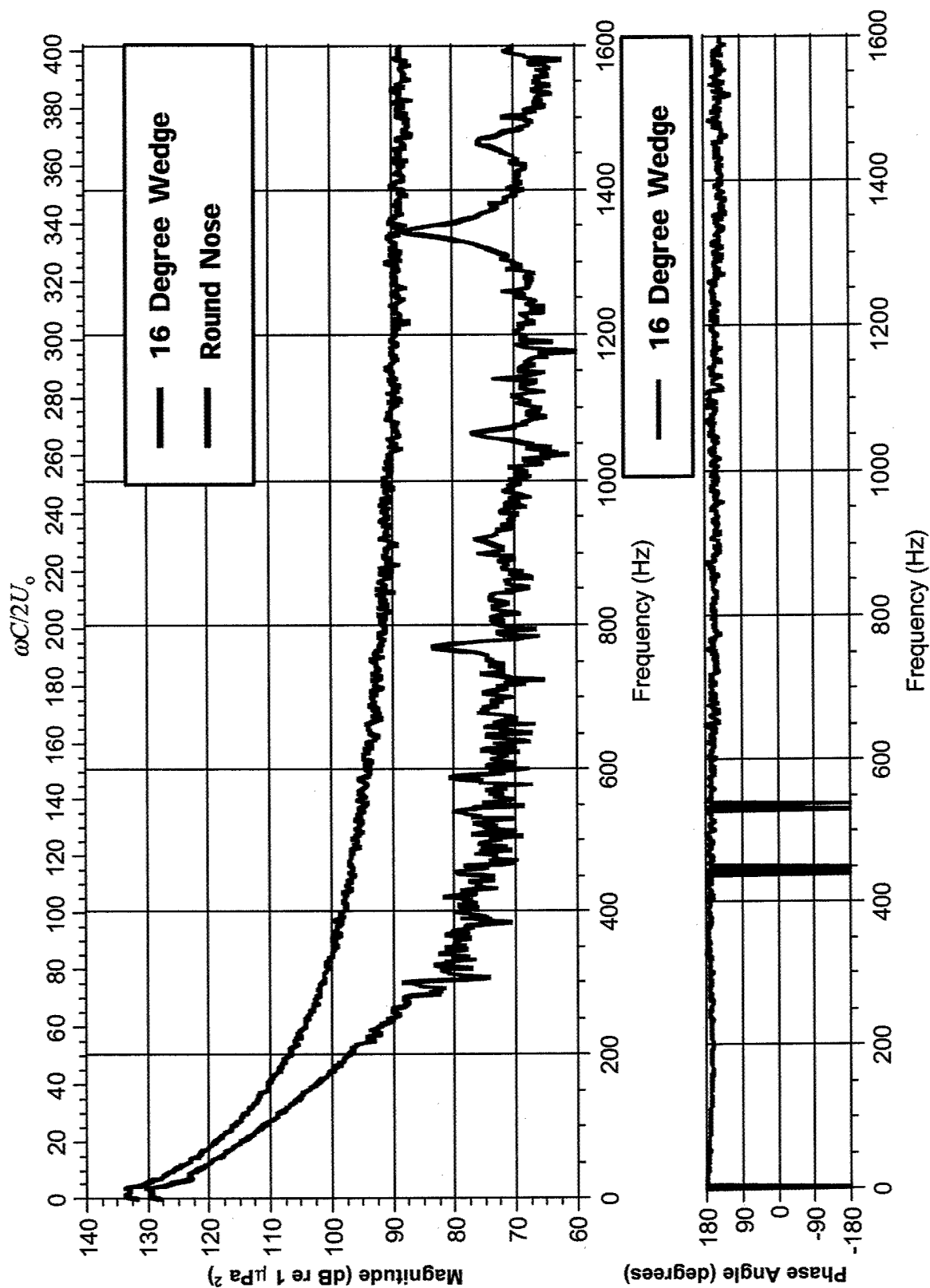


Figure 3.12. Cross power spectrum magnitude and phase from pressures measured on opposite sides of the foil near the leading edge of the round nose (RN) and the 16 degree wedge (SN) at $U_o = 50$ ft/s.

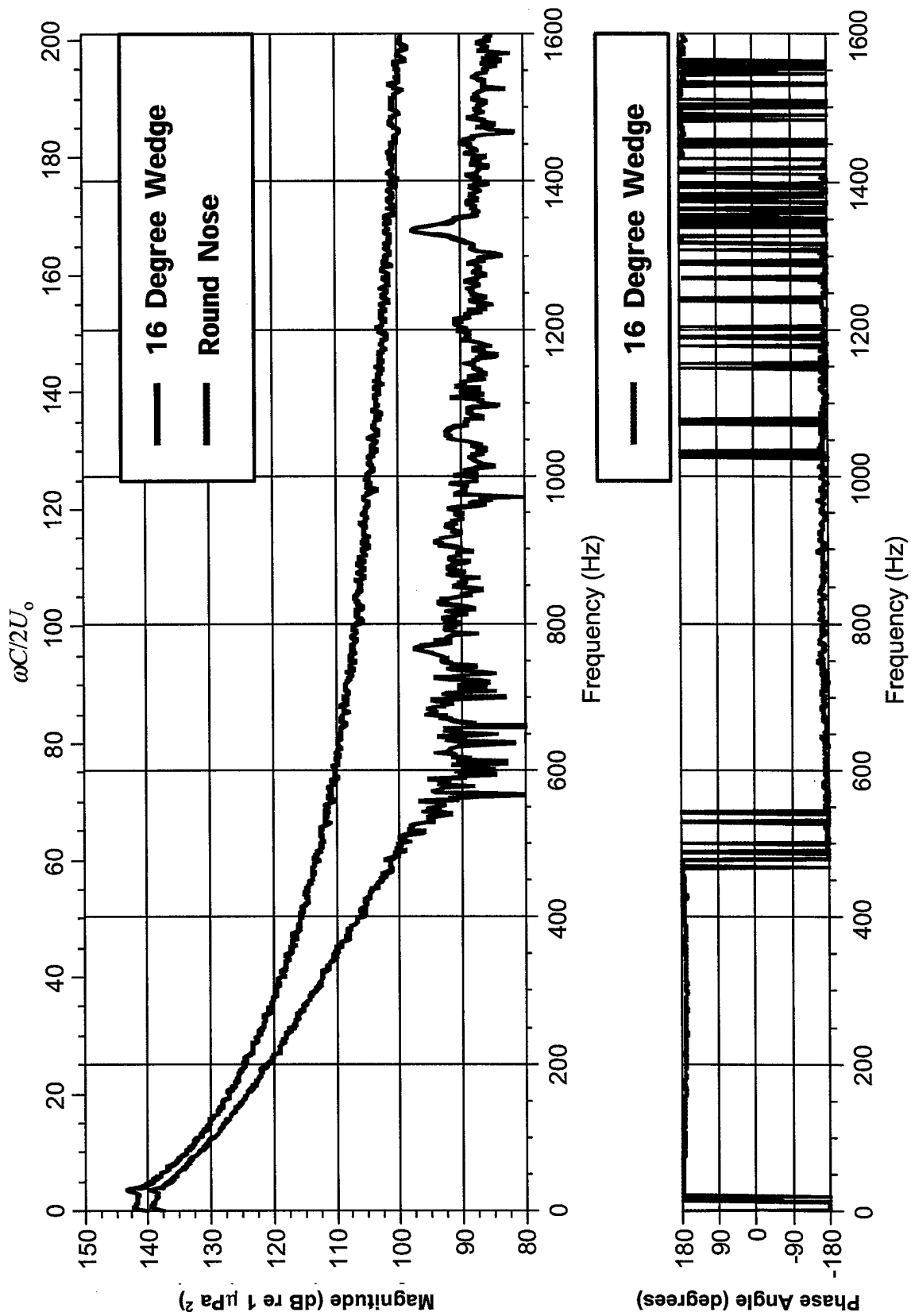


Figure 3.13. Cross power spectrum magnitude and phase from pressures measured on opposite sides of the foil near the leading edge of the round nose (RN) and the 16 degree wedge (SN) at $U_0 = 100$ ft/s.

4. Conclusions

Surface pressure cross spectra were used to dissect the contributions from the acoustic near field pressures of the leading edge lifting dipoles and the quadrupoles of the grid-generated turbulence that served as the incident field. Coherence measurements of the surface pressure spectra made on opposite sides of the leading edge confirm that the scattered field is uncoupled to the $\phi(k_2)$ components of the incident turbulence. This is exploited with the use of cross spectral measurements on opposite sides of the foil to reject the incident fields so that the scattered surface pressures can be measured at higher frequencies where the thickness effect is pronounced. The surface pressure cross spectra showed the thickness correction to Sears' function [Gershfeld (2003)] that was also observed in the far field from the dipole sound measurements of Paterson and Amiet (1976, 1977) and Olsen and Wagner (1982). The thickness dependence of the dipole sound is only weakly dependent on the leading edge radius of curvature at the apex of the edge and is mainly a function of the foil's maximum section thickness.

References

- Amiet, R.K., "Acoustic Radiation from an Airfoil in a Turbulent Stream," J. Sound and Vib. 41(4), pp. 407-420 (1975).
- Corcos, G.M., "The resolution of pressure in turbulence," J. Acoust. Soc. Am. 35, pp. 192-199 (1963).
- Crighton, D.G. and Leppington, F., "Scattering of Aerodynamic Noise by a semi-infinite compliant plate," J. Fluid Mech. 71, pp. 625-673 (1975)
- Gershfeld, J.L., "Leading Edge Noise from Thick Foils in Turbulent Flows", NSWCCD-72—TR-2003/099, September 2003.
- Grace, S.M., "Unsteady blade response: the BVI model vs. the gust model," AIAA 2001-2209, 7th AIAA/CEAS Aeroacoustics Conference, May 28-30, 2001/ Maastricht, The Netherlands (2001).
- Howe, M.S., "The Influence of Surface Rounding on Trailing Edge Noise," J. Sound and Vib. 126, No. 3, pp.503-523 (1988).
- Howe, M.S., Acoustics of Fluid-Structure Interactions, 1st ed., Cambridge University Press, (1998a).
- Howe, M.S., "Reference Manual on the theory of lifting surface noise at low Mach numbers," Boston Univ. Report AM-98-001 (1998b).
- Martinez, R. and Rudzinsky, J., "Analytic Evaluation of Shape effects on blade-vortex interaction," CAA Report U-2466-402.14 (Dec. 1997).
- Minniti III, R.J. and Mueller, T.J., "Experimental Investigation of Unsteady Aerodynamics and Aeroacoustics of a Thin Airfoil," AIAA J. 36, No. 7, pp. 1149-1156 (1998).
- Olsen, W. and Wagner, J., "Effect of Thickness on airfoil Surface Noise," AIAA 82-4068 (1982).
- Osborne, C., "Unsteady Thin-Airfoil Theory for Subsonic flow," AIAA J. 11, No. 2, pp. 205-209 (1973).
- Paterson, R.W. and Amiet, R.K., "Noise and Surface Pressure Response of an Airfoil to Incident Turbulence," NASA CR-2733 (Sept. 1976).
- Paterson, R.W. and Amiet, R.K., "Noise and Surface Pressure Response of an Airfoil to Incident Turbulence," J. Aircraft 14, No. 8, pp. 729-736 (1977).
- Sears, W. R., "Some aspects of non-stationary airfoil theory and its practical applications." J. Aeronautical Sci. 8, pp. 104-108 (1941).

INITIAL DISTRIBUTION (U)
DIVISION DISTRIBUTION

Organization	Code	Name	Code	Name
NAVSEA			508	Brown
PEO-SUB-RT1		Stout	508	Cox
05H		Crockett		
			70	
ONR				
ONR 334		Kim	7020	Strasberg
DTIC			7051	Blake
			7052	Feit
			7053	Liu
			713	Mathews
			72	Shang
			722	Hughes
			725	Noll
			725	Farabee
			725	Gershfeld (5 copies)
			725	Goody
			725	Lynch
			725	Maga
			725	Roth
			725	Wojno
			725	Zawadzki
			725	Zoccola